Interface passivation using ultrathin polymer-fullerene films for high-efficiency perovskite solar cells with negligible hysteresis†

Jun Peng,*[a] Yiliang Wu,[a] Wang Ye,[b] Daniel Jacobs,[a] Heping Shen,[a] Xiao Fu,[a] Yimao Wan,[a] The Duong,[a] Nandi Wu,[a] Chog Barugkin,[a] Hieu Nguyen,[a] Dingyong Zhong,[b] Juntao Li,[b] Teng Lu,[c] Yun Liu,[c] Mark N. Lockrey,[d] Klaus J. Weber,[a] Kylie R. Catchpole,[a] Thomas P. White*[ab]

Interfacial carrier recombination is one of the dominant loss mechanisms in high efficiency perovskite solar cells, and has also been linked to hysteresis and slow transient responses in these cells. Here we demonstrate an ultrathin passivation layer consisting of a PMMA:PCBM mixture that can effectively passivate defects at or near to the perovskite/TiO_2 interface, significantly suppressing interfacial recombination. The passivation layer increases the open circuit voltage of mixed-cation perovskite cells by as much as 80 mV, with champion cells achieving V_{oc} ~1.18 V. As a result, we obtain efficient and stable perovskite solar cells with a steady-state PCE of 20.4% and negligible hysteresis over a large range of scan rates. In addition, we show that the passivated cells exhibit very fast current and voltage response times of less than 3 s under cyclic illumination. This new passivation approach addresses one of the key limitations of current perovskite cells, and paves the way to further efficiency gains through interface engineering.

Broader context

Metal halide perovskite solar cells have attracted tremendous attention and rapidly risen to the forefront of the emerging photovoltaic technologies in the past five year. However, most perovskite solar cells reported so far still suffer from low open-circuit voltage well below the theoretical limit (~1.33 V). Several recent studies have identified carrier recombination at the perovskite/transport layer interfaces as being the dominant loss mechanism in high-efficiency perovskite cells, resulting from localized defects/trap states at the interfaces. Interface recombination and trapping also contributes to the commonly-observed hysteresis and slow transient responses of many perovskite cells. Therefore, rational interface passivation techniques are critical for further boosting the performance of perovskite solar cells. In this work, we demonstrate the use of ultrathin polymer-fullerene blend films as passivation layers to effectively suppress interface recombination at the perovskite/electron transport layer interface. This approach successfully addresses one of the key limitations of the perovskite solar cells, and paves the way to boost its efficiencies beyond 22%.

Introduction

Solution-processed hybrid organic/inorganic perovskite solar cells have achieved certified power conversion efficiency (PCE) of over 22%[1] within seven years' development, and are regarded as promising candidates for next-generation thin-film solar cells.[2-8] State-of-the-art perovskite solar cells use mixed-cation perovskite compositions with a sandwich structure of ETL/perovskite/HTL, where ETL and HTL are the electron transport layer and hole transport layer, respectively.[3-5] To date numerous organic and inorganic HTLs and ETLs with suitable work functions and high charge mobility have been developed to improve the energy level alignment and to facilitate charge extraction, with the ultimate aim of enhancing the PCE of perovskite solar cells.[9-14] However, most perovskite solar cells reported so far suffer from a relatively low open-circuit voltage (V_{oc}) (well below the theoretical limit of ~1.33 V),[2,13,15,16] and current-voltage (*J-V*) hysteresis. Recent studies suggest that both of these major issues are related to the presence of defects and trap states at the perovskite/ETL and/or perovskite/HTL interfaces.[3,9,17-19] Interfacial carrier recombination impacts perovskite photovoltaic performance, leading to reduced carrier lifetimes, and voltage loss.[3,17] Furthermore, the combination of ion migration in the perovskite film, and interfacial recombination is thought to be responsible for many of the observed hysteresis behaviours.[20-22] Consequently, rational interface passivation techniques are critical for further improving the performance of perovskite solar cells.[3,23,24]

There are three main approaches for reducing the impact of interfacial recombination in perovskite solar cells. The first is to reduce the host materials' defect density by adding dopants.[4,9,13,15,25-27] For example, Giordano *et al.*[9] demonstrated lithium doping of TiO_2 ETLs as a way to passivate trap states within the TiO_2 lattice, increasing V_{oc} from 1.04 V to 1.114 V, and producing cells with negligible hysteresis. Saliba *et al.*[4] reported a perovskite solar cell with a stabilized PCE of 21.6% and an impressive V_{oc} of 1.18 V by incorporating the Li-doped *meso*-TiO_2 scaffold and Rb-containing perovskite. The second approach is to use alternative transport layer materials that have lower defect densities and/or form better quality interfaces to perovskite.[10,11,17,28-33] For example, Correa Baena *et al.*[29] and Wang *et al.*[30] replaced the commonly-used TiO_2 ETL with SnO_2 and achieved reduced hysteresis and V_{oc} values of 1.14 V and 1.12 V, respectively. Correa Baena *et al.*[17] also showed that reducing the doping concentration of the Spiro-OMeTAD (2,2',7,7'-Tetraakis-(N,N-di-4-methoxyphenylamino)-9,9'-spirobiflu-orene) HTL can suppress interfacial recombination, producing a stabilized PCE of approx. 20% with V_{oc}=1.17 V.

The third approach to reduce interfacial recombination is to introduce a very thin passivation layer between the perovskite and transport layers.[18,19,34-39] For example, Zhang *et al.*[35] showed that a very thin fullerene derivative (α-bis-PCBM) layer between the perovskite and the Spiro-OMeTAD HTL can reduce cell degradation and passivate defects at the perovskite/HTL interface, yielding a PCE of 20.8%, and V_{oc}= 1.13 V. Similarly, Koushik *et al.*[37] and Wang *et al.*[39] used ultrathin layers of Al_2O_3 and poly(methyl methacrylate) (PMMA) respectively to passivate the perovskite/Spiro-OMeTAD interface, resulting in improved V_{oc} (1.08V and 1.06V respectively) and reduced hysteresis. Recently,

Tan *et al.*[3] reported that chlorine-capped TiO_2 colloidal nanocrystal ETLs can mitigate interfacial recombination and improve interface binding, resulting in a high V_{oc} of 1.189 V, a certified PCE of 20.1%, and negligible hysteresis. While these examples show that reducing interface recombination is crucial for improving V_{oc} and cell efficiency, only a very small number of interfacial passivation methods reported so far have produced cells with V_{oc} >1.15V,[3,4,17,28] and even the best perovskite cells still have voltages well below the theoretical limit.[2-7,15,25,40,41] Hence, there is a clear need to develop new interface passivation approaches to realize the full potential of perovskite photovoltaics.

In this work, we use very thin layers of PMMA:PCBM mixtures to suppress interfacial recombination at the perovskite/mesoporous-TiO_2 interface of high-efficiency mixed-cation perovskite cells. We show that PMMA provides exceptional passivation, increasing V_{oc} by up to 80 mV, but at the expense of conductivity (and hence fill factor (FF)). However, the addition of PCBM to the film allows us to tune the passivation/conductivity (V_{oc}/FF) trade-off to maximize efficiency, resulting in a cell with a steady-state PCE of 20.4%, V_{oc} = 1.16V and negligible hysteresis. We further show that the passivated cells have some of the fastest transient responses reported to date; reaching steady-state conditions less than 3s after illumination, compared to more than 40s for control cells.

Results and discussion

To evaluate the passivation performance of ultrathin PMMA:PCBM (less than 5 nm, estimated from the profile atomic force microscopy (AFM) measurement, see Fig. S1, ESI†) films at the perovskite/ETL interface, we prepared cells with six different conditions: a control cell (no passivation layer), and cells with PMMA:PCBM ratios (w/w) of 1:0 (pure PMMA), 1:1, 1:3, 1:5 and 0:1 (pure PCBM). All other cell fabrication steps were kept the same and more than 20 cells were prepared for each condition. The final device structure was FTO/*c*-In-TiO_x (~70 nm)/*m*-TiO_2 (~110 nm)/Passivation layer/Perovskite (capping layer ~480 nm)/Spiro-OMeTAD (~160 nm)/Au (Fig. 1a and 1b), where *c*-In-TiO_x and *m*-TiO_2 represent compact indium-doped TiO_x layer[27] and mesoporous TiO_2 layer, respectively; and perovskite stands for $Cs_{0.07}Rb_{0.03}FA_{0.765}MA_{0.135}PbI_{2.55}Br_{0.45}$.

To ensure that the composition and quality of the perovskite film is not influenced by the underlying passivation layer, we investigated the deposited perovskite films using X-ray diffraction (XRD) and scanning electron microscopy (SEM). The XRD spectra show no systematic variations with substrates, and no obvious PbI_2 or other non-perovskite phases, as well as no significant variation in crystallite size (see Fig. S2, ESI†). We also observe no significant differences in the top-morphology of the pinhole-free and uniform perovskite films on different substrates in SEM images (see Fig. S3, ESI†). In addition, the evidence from backscattered electron (BSE) imaging measurements and energy dispersive X-ray (EDX) analysis further support our XRD and SEM results (see Fig. S4 and S5, ESI†). From these results we conclude that the bulk quality of the perovskite films is unaffected by the passivation layer, and will be the same in all of the control and passivated cells.

The performance characteristics and distribution of results for each cell condition are plotted in Fig. 1c-f. Fig. 1c shows a dramatic increase in V_{oc} from 1.08 V (mean V_{oc}) for the control cells to ~1.16 V (mean V_{oc}) for the cells with a pure PMMA passivation layer at the *m*-TiO_2/perovskite interface. The highest V_{oc} for these cells was ~1.18 V. We attribute this significant improvement to the excellent passivation properties of the PMMA, which has previously been used to passivate the perovskite/HTL interface,[39] and has also been shown to passivate surface trap states and suppress hysteresis in ZnO field-effect transistors and quantum-dot light-emitting devices.[42,43] Although the exact passivation mechanism in our cells is unclear, previous work suggests that the PMMA could serve a double-passivation role, reducing defects on both the perovskite and TiO_2 surfaces. On the ETL side, the cross-linked PMMA film protects the TiO_2 surface from oxygen adsorption which can cause depletion of surface electrons and increased recombination.[39,43] At the same time, the PMMA may also passivate defects/deep trap centres caused by the dangling bonds (under-coordinated lead ions or iodine terminations) localized at the perovskite surface, as has been suggested by Kong *et al.*[44] This latter passivation mechanism is similar to that already reported for PCBM[18] and thiophene/pyridine.[45]

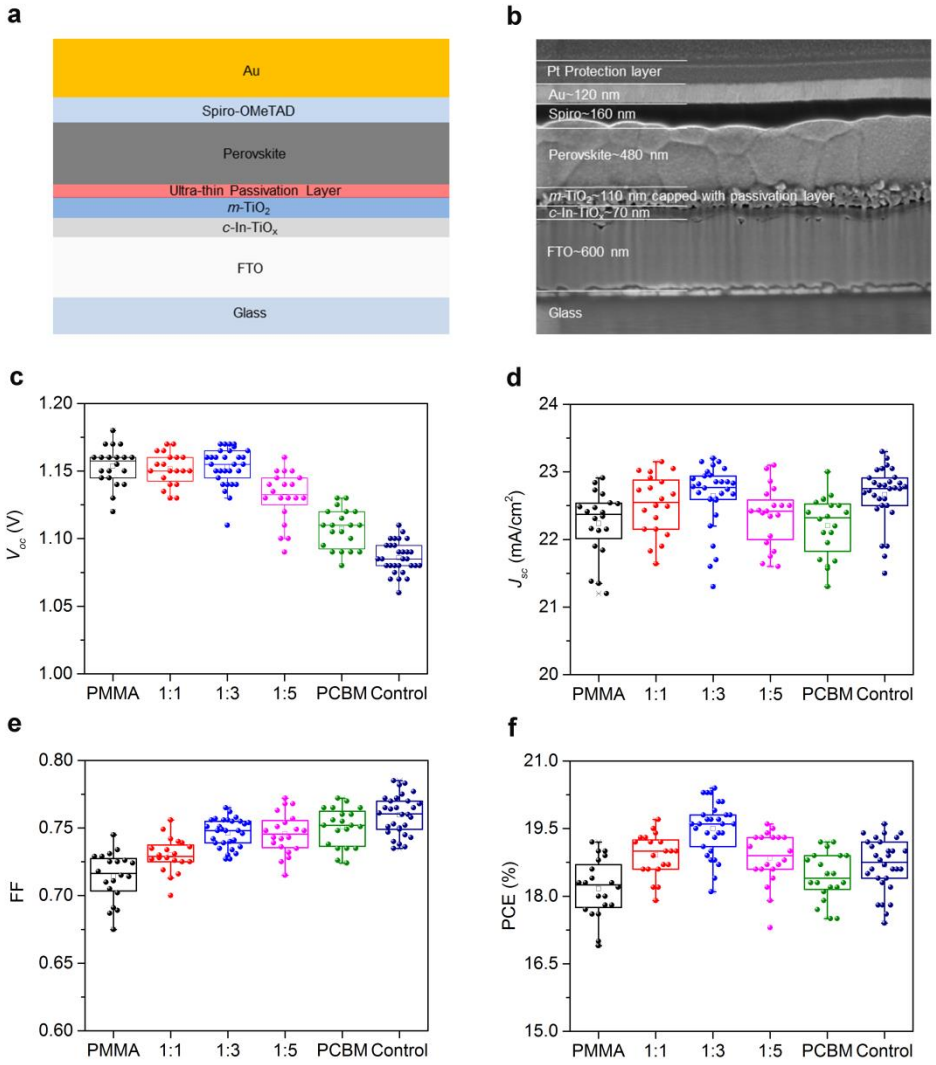

Fig. 1 a) Schematic of the standard device structure. b) SEM cross-section of a perovskite solar cell with the structure FTO/*c*-In-TiO_x/*meso*-TiO_2/Passivation layer/Perovskite/Spiro/Au. The perovskite composition is $Cs_{0.07}Rb_{0.03}FA_{0.765}MA_{0.135}PbI_{2.55}Br_{0.45}$. c)-f) Statistical distribution of the photovoltaic parameters for cells with/without PMMA, PMMA:PCBM, and PCBM passivation layer: c) distribution of V_{oc}; d) distribution of J_{sc}; e) distribution of FF; f) distribution of PCE. Note that the Pt protection layer seen in b) was only used to prepare the focused ion beam (FIB) SEM cross-sectional image. Results are shown for 140 cells (30 cells for the control and 1:3, and 20 cells for the others) collected from 4 different batches. All devices were tested at a 50 mV/s reverse scan rate.

As expected, the mean value of FF for the pure PMMA cells was lower than that of the control cells, due to the increased series resistance of the non-conducting PMMA (Fig. 1e). Accordingly, we mixed PCBM, an n-type organic material with a good electron mobility,[46] into the PMMA to form PMMA:PCBM blend films in an attempt to reduce the series resistance. The role of the PCBM as an additive in increasing the conductivity of PMMA:PCBM blend films was confirmed by conductive atomic force microscopy (C-AFM) measurements (see Fig. S6, ESI†). As can be seen in Fig. 1c, The mean V_{oc} values (~1.16 V) for the cells with PMMA:PCBM ratios of 1:1 and 1:3 show negligible difference compared to the cells passivated with pure PMMA. However, a decreased V_{oc} (mean ~1.13 V) was observed for a PMMA:PCBM ratio of 1:5. Fig. 1e shows that the FF increases with PCBM content, as expected from an increase in the passivation layer's conductivity. The cell with the pure PCBM passivation layer also showed an increased V_{oc} (~1.11V) relative to the control cell, consistent with previous reports that PCBM can passivate perovskite grain boundaries and reduce defects/trap states at or near perovskite interfaces.[18,19,47] The voltage improvement, however is significantly lower than for the optimum PMMA:PCBM blend, indicating the superior passivation properties of PMMA in this situation.

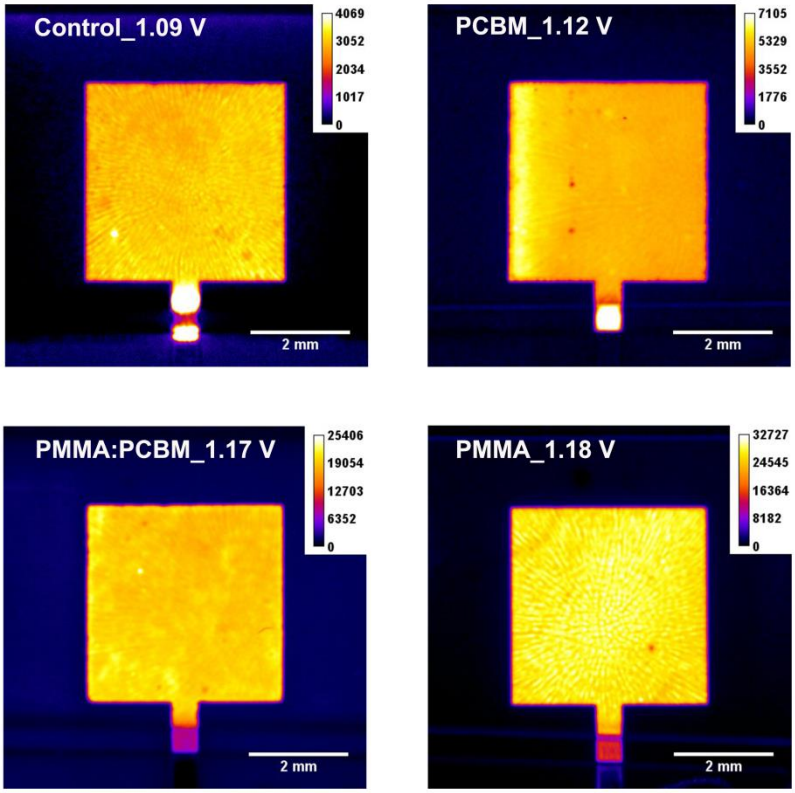

Fig. 2 Photoluminescence (PL) images of a control (no passivation layer) cell and cells with PCBM, PMMA:PCBM (1:3), and PMMA passivation layers.

We next consider the short-circuit current density (J_{sc}), which also shows some dependence on the passivation layer, although much less significant than for the V_{oc} and FF. Since the perovskite and HTL layers in each cell should be identical, one possible origin of J_{sc} differences is the optical properties of the passivation layer. Therefore, we measured the transmittance of the substrates prepared with the different passivation layers (see Fig. S7, ESI†). As expected, the transmittance of the sample with the pure PMMA film is almost identical to the control sample due to the large optical transmittance, with the highest losses at visible wavelengths where PCBM is known to be absorbing and is widely used as an acceptor in organic solar cells.[48] As expected, the transmittance of the PMMA:PCBM samples decreases with increasing PCBM content. Fig. 1d shows that the measured J_{sc} of the control cell, and the cells passivated with pure PCBM and PMMA:PCBM ratios of 1:3 and 1:5 follow the trends predicted by the transmittance data, with the control cell having the highest mean J_{sc} (~22.7 mA/cm^2), and the PCBM cell having the lowest (22.2 mA/cm^2). We note, however,

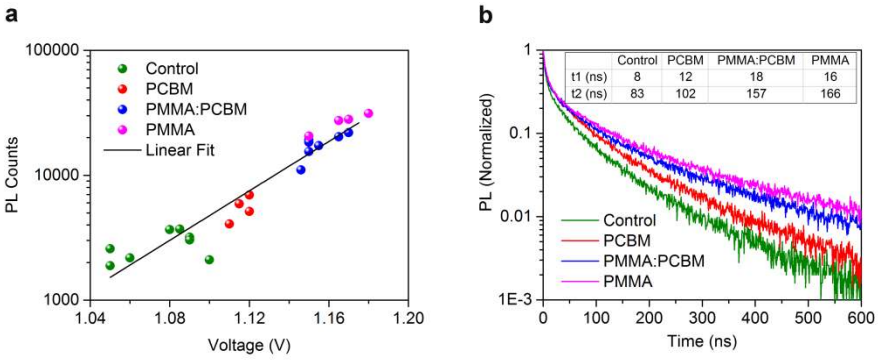

Fig. 3 a) Logarithmic plot of PL intensity *vs* V_{oc}. b) Time-resolved photoluminescence (TRPL) decay measurements for the perovskite thin films on FTO/*c*-In-TiO$_x$/*m*-TiO$_2$ substrates with/without PCBM, PMMA:PCBM (1:3) or PMMA passivation layer.

bandgap of the PMMA. The pure PCBM sample had the lowest that the Jsc reduces slightly again with increasing PMMA ratio; the

cell with the 1:1 PMMA:PCBM passivation layer has a lower J_{sc} than the 1:3 ratio cell, and the cell with the pure PMMA film has a J_{sc} similar to the pure PCBM cell. This trend cannot be explained by the transmittance measurements and most likely results from a slight reduction in carrier collection efficiency, the origin of which is not yet known.

The combined effect of the observed trends in V_{oc}, FF and J_{sc} can be seen in Fig. 1f, which shows the PCE distributions for each cell condition. From this figure it is clear that the optimum ratio of PMMA:PCBM is 1:3, resulting in a mean PCE of 19.5%; corresponding to an absolute efficiency gain of 1.1% compared to that of the control cells (mean PCE 18.4%).

The energy band alignment at the perovskite/ETL interface is another important parameter that can influence open circuit voltage. To investigate this possibility further, we measured the work function of FTO/*c*-In-TiO$_x$/*m*-TiO$_2$ and FTO/*c*-In-TiO$_x$/*m*-TiO$_2$/PMMA:PCBM samples with different blend ratios using ultraviolet photoelectron spectroscopy (UPS). As shown in Fig. S8 (ESI†), the WF of FTO/*c*-In-TiO$_x$/*m*-TiO$_2$/PMMA (~3.97 eV) shows only a 30 meV shift relative to the control FTO/*c*-In-TiO$_x$/*m*-TiO$_2$ (~4.0 eV) sample, while the FTO/*c*-In-TiO$_x$/*m*-TiO$_2$/PCBM has a 60meV shift (~3.94 eV). Predictably, samples with PMMA:PCBM blends show WF shifts of 40-50meV relative to the control. Given the relatively small changes in WF and the lack of obvious correlation with measured V_{oc} we infer that the shift in WF with the addition of the ultrathin films is not a dominant contribution to the improved cell performance.

To further characterize the passivation performance of the PMMA:PCBM layers, we also investigated the photo-luminescence (PL) intensity of four different complete cells using PL imaging under open-circuit condition (see Fig. 2). As expected, the cells with the highest V_{oc} have the highest PL intensity. In an ideal cell at T=300 K, the steady-state PL intensity will increase by tenfold if the open circuit voltage increases by ~60 mV.[49-51] A logarithmic plot of PL intensity *vs* V_{oc} (Fig. 3a) shows a clear linear relationship for our cells, with a slope of ~101 mV/decade. This higher value than the theory may result from a potential barrier at one or both interfaces causing ion accumulation, as has been reported previously.[51] Another possibility is energy level misalignment at the perovskite/ETL and/or perovskite/HTL interfaces contributing to V_{oc} loss, especially in the samples with higher interfacial recombination. Nevertheless, the clear logarithmic relationship between PL intensity and V_{oc} across multiple cells is notable given that few papers have shown this trend before for perovskite cells.

Defect related recombination can normally be divided into bulk and interface defects. The bulk defects within perovskite absorber are not expected to change with the addition of the passivation layers given the XRD and SEM observations discussed earlier. Therefore, the more than six-fold increase in PL intensity for our best passivated cells suggest that the surface recombination at or near to the perovskite/ETL interfaces is significantly supressed by the addition of the thin PMMA:PCBM film.

The steady-state PL results are supported by time-resolved photoluminescence (TRPL) decay measurements. Transient PL curves for perovskite thin films on FTO/*c*-In-TiO$_x$/*m*-TiO$_2$ substrates with/without PCBM, PMMA:PCBM (1:3) or PMMA passivation

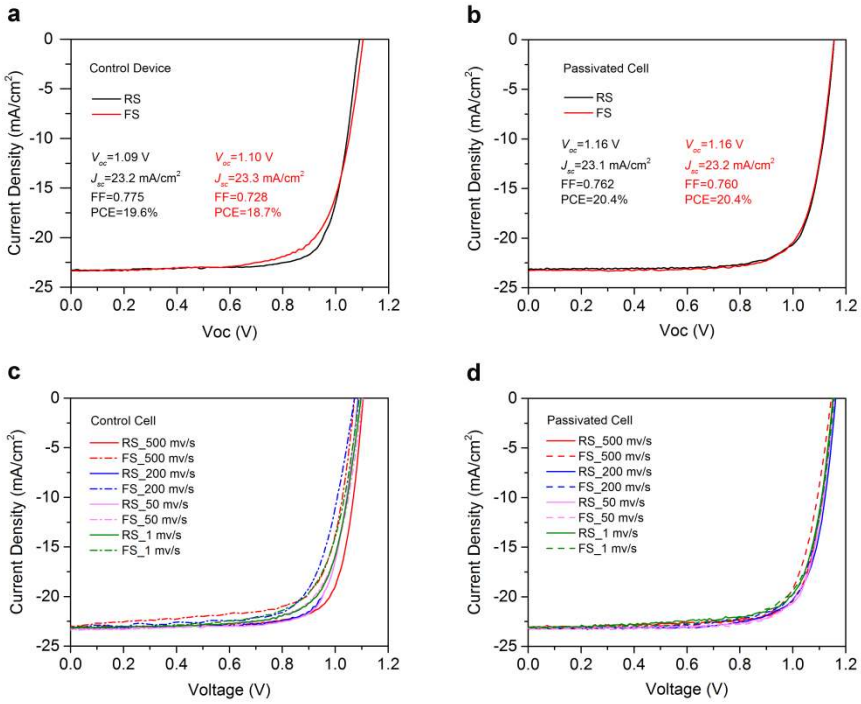

Fig. 4 Photovoltaic parameters of champion control and passivated cells. a) Current density-voltage curves of the control cell. b) Current density-voltage curves of the passivated cell with PMMA:PCBM (1:3) passivation layer. c) Current density-voltage curves of the control cell measured at different scan rates. d) Current density-voltage curves of the passivated cell measured at different scan rates. Note that the legend label RS represents reverse scan (from V_{oc} to J_{sc}), and the FS represents forward scan (from J_{sc} to V_{oc}).

layer are plotted in Fig. 3b, showing a much slower PL decay for the passivated samples compared to the un-passivated control. A bi-exponential model in the decay analysis software was used to fit the PL decay data and extract the lifetimes shown in the table inserted in the Fig. 3b. The control sample has a fast decay lifetime τ_1 = 8 ns and a slow decay lifetime τ_2 = 83 ns. In contrast, the perovskite thin films with the PMMA:PCBM (or PMMA) passivation layers have a τ_1 = 18 ns (16 ns) and τ_2 = 157 ns (166 ns), respectively. The lifetimes of the pure PCBM coated samples lie between these samples and the control. We therefore find that both the fast and slow PL lifetime components increase as a result of the passivation. These observations further support our conclusions from the full cell results and steady-state PL measurements that the ultra-thin PMMA:PCBM film effectively reduces non-radiative recombination at the perovskite/ETL interface by reducing the density of defects and trap states, resulting in the dramatic increase in open-circuit voltage. In addition, the evidence from space charge limited current (SCLC) measurements for our passivated and non-passivated cells may further support our findings obtained from the steady-state PL and transient PL measurements.(see Fig S9, ESI†)

Fig. 4 shows the performance of our champion control and passivated cells. The control cell, without a passivation layer, has a PCE of 19.6%, V_{oc}=1.09 V, J_{sc}=23.2 mA/cm^2 and FF=0.775 obtained from a reverse *J-V* scan at 50 mV/s scan rate (see Fig. 4a). However, due to some hysteresis, the efficiency is ~0.9% lower when measured by a forward scan at the same rate. In contrast, the cell with the PMMA:PCBM (1:3) passivation layer shows negligible hysteresis between reverse and forward *J-V* scans at 50 mV/s scan rate, achieving a PCE of 20.4%, V_{oc}=1.16 V, J_{sc}=23.1 mA/cm^2 and FF=0.762 (see Fig. 4b). Integrated current densities from the measured external quantum efficiency (EQE) spectra of both control and passivated cells are within 6% of the J_{sc} values extracted from the *J-V* curves (see Fig. S10, ESI†). Note when comparing the transmission data (Fig. S7, ESI†) and EQE data (Fig. S10, ESI†) that the reflection of FTO/*c*-In-TiO$_x$/*m*-TiO$_2$/Mixed-cation Perovskite/Spiro-OMeTAD/Au is lower than that of FTO/*c*-In-TiO$_x$/*m*-TiO$_2$, due to the more gradual change of refractive index of the layers within the structure, as well as the absorption within the perovskite for wavelengths below 750nm.

Steady-state efficiencies measured at the maximum power point voltage (V_{mpp}) for both control and passivated cells are also provided in Fig. S11 (ESI†). The steady-state efficiency of 18.5% for the control cell is 1.1% lower than the value obtained from the *J-V* scan due to hysteresis effects. For the passivated cell, however, the steady-state PCE (20.4%, tested at 0.97 V) matches exactly the PCE measured from both the reverse and forward *J-V* scans.

To further demonstrate the very low hysteresis of our passivated cells, we measured the cells at different scan rates varying from fast (500 mV/s) to very slow (1 mV/s). As shown in Fig. 4c and 4d, we found that the hysteresis of the control cell gets worse when tested at fast scan rates of 200 mV/s and 500 mV/s, or very slow scan rates of 1 mV/s. On the other hand, the passivated cell shows negligible hysteresis between reverse and forward scans under different scan rates. The detailed performance parameters of the control cell and passivated cell are also provided in Table S1 (ESI†) and Table S2 (ESI†). We also summarize in Table S3 (ESI†) the performance parameters of the best n-i-p perovskite cells reported in the literature so far with efficiencies above 20 %.

The low hysteresis in the passivated cells is a direct consequence of the very rapid response times of these cells, as seen in transient V_{oc} and J_{sc} measurements under light/dark cycling (Fig. 5). This data was obtained in the following way: first, fresh cells were kept in the dark with no pre-conditioning, until the V_{oc} (or J_{sc}) was stable (V_{oc} ~ 0, or J_{sc} ~ 0) for 100 s; next, the light (solar simulator, one sun intensity) was switched on and the V_{oc} (or J_{sc}) was tracked over time

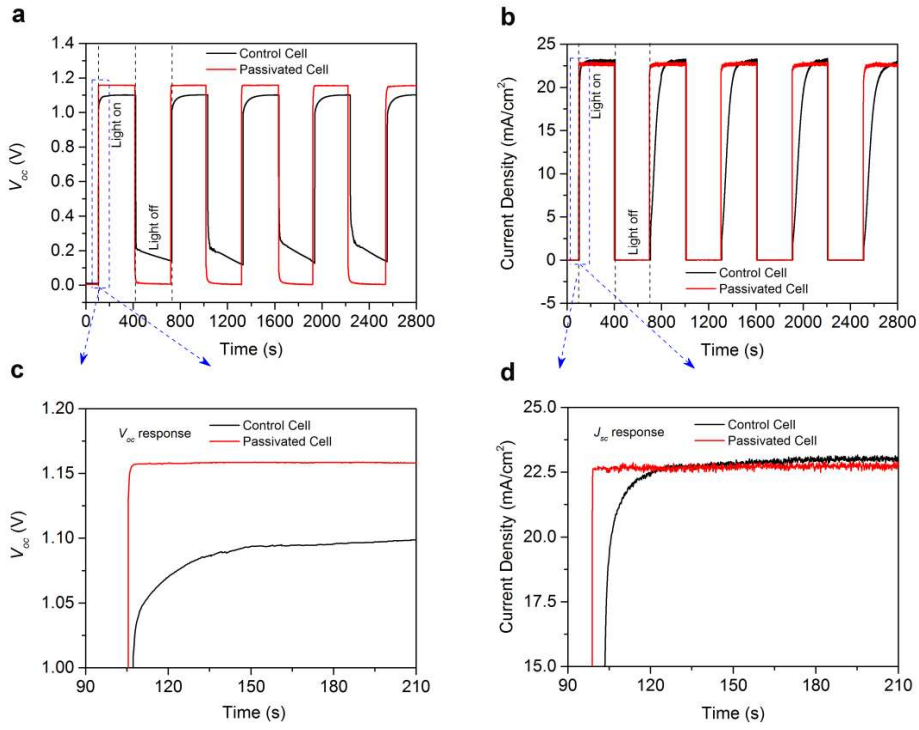

Fig. 5 V_{oc} and J_{sc} response tests for control and passivated cells under cyclic illumination. a,c) V_{oc} response; b,d) J_{sc} response . Note that c) and d) are zoomed-in versions of a) and b), respectively.

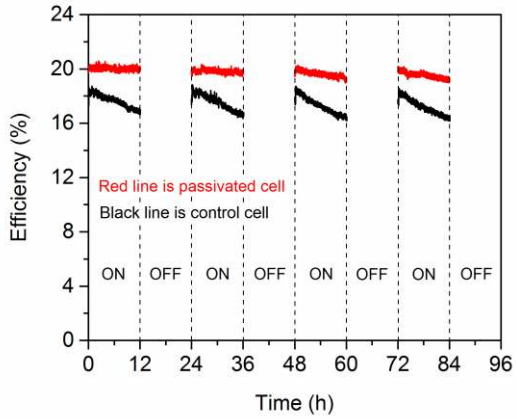

Fig. 6 The stability of the control cell and passivated cell under four cycles of 12 hr illumination (on)/12 hr dark (off).

until the it reached a steady value (maximum V_{oc} or J_{sc}); finally the light was switched off and the V_{oc} (or J_{sc}) was tracked for another 300 s. This was repeated four more times (Fig. 5).

As shown in Fig. 5, the passivated cell exhibits a much faster response than the control cell. Zooming on the first dark/light transition (Fig. 5a and 5c) reveals that the V_{oc} of the passivated cell reaches a steady-state maximum in less than 3 s. In contrast, the control cell took around 40 s for the V_{oc} to stabilize. There is also a significant difference in response when the light is switched off: while the V_{oc} of the passivated cell rapidly drops back to 0 V, the V_{oc} of the control cell initially drops rapidly to 0.2 V, and then decreases much more slowly to ~0.1 V after 300 s. As a consequence of this slow voltage decay, the response of the control cell to the first illumination cycle is different to the second and subsequent cycles, whereas the response of the passivated cell is the same on each cycle.

There are a number of possible explanations for the difference in transient behaviour of the control and passivated cells, two of which are the slow release of trapped ions or charge carriers. Several sources have suggested that ion trapping at the TiO_2 interface may contribute to the slow response time of cells prepared on TiO_2 substrates.[52,53] The availability of ionic traps would be greatly reduced by the passivation layers, so that fewer ions are trapped and released, resulting in a much faster response. Alternatively, the voltage transient at the end of the illumination cycle may be due to injection of carriers into the perovskite[54] from interfacial defects that become filled with carriers (electrons or holes) during illumination. When illumination is turned off, these carriers may de-trap over timescales of seconds leading to a transient voltage.[54] Again, passivation of the interface would reduce the trapped carrier concentration, leading to a faster transient response. We stress, however, that there are several other possible mechanisms responsible for the transient voltage decay, and further work would be required to establish the exact cause.

The dark/light J_{sc} response for the cells with/without PMMA:PCBM passivation layer are also provided in Fig. 5b and 5d. Similarly to the V_{oc}, the J_{sc} response of the passivated cell shows a much smaller delay than the control cell. These very rapid V_{oc} and J_{sc} response rates are some of the fastest ever reported for perovskite cells.[4,17,25,28]

We have also conducted 12 hr light/dark cycling to simulate day/night operation of the cells as shown in Fig. 6. In these tests the cells were held at the V_{mpp} during the light part of the cycle, and open circuit during the dark part of the cycle. Impressively, the steady-state PCE of the passivated cell exhibits an excellent stability (the steady-state PCE~19.4%) under continuous operation at V_{mpp} after four cycles of the 12-hour-light/dark test compared to the control cell which dropped in efficiency from 18.5% to 16.2%. This suggests that the passivation layer may also protect the cells from degradation associated with repeated light/dark cycling, perhaps by reducing the availability of ion trapping sites.[55]

Conclusions

We have shown that ultrathin PMMA:PCBM blend films can effectively passivate the perovskite/*m*-TiO_2 interface of high efficiency perovskite cells, leading to a significant reduction in interfacial recombination and a dramatic increase in V_{oc} from 1.1 V (control cell) to 1.18 V (passivated cell). By optimizing the PMMA:PCBM ratio to achieve both high V_{oc} and fill-factor we obtained stable perovskite solar cells with a steady-state PCE of 20.4% and negligible hysteresis. The optimized cells also exhibit an exceptionally rapid current and voltage response when illuminated, reaching steady-state V_{oc} or J_{sc} in less than 3s. This new passivation approach addresses one of the main limitations of current high-efficiency perovskite solar cells - interface recombination - and demonstrates the potential for ultrathin passivation layers to significantly improve cell performance. Furthermore, our finding that pure PMMA films provided the best passivation, but insufficient conductivity, indicates the potential for further improvements if new n-type polymer materials can be developed with appropriate band alignment and carrier mobility.

Author contribution

J.P. conceived and designed the overall experiments. J.P., Y.W., H.S., T.D., N.W. and D.J. prepared and characterized the perovskite cell devices. Y.W. and N.W. conducted the PL imaging measurements and analysis. W.Y., D.Z. and J.L. conducted the XPS/UPS measurements and analysis. X.F. and H.N. performed the TRPL measurements and analysis. H.S. and T.D. conducted the XRD and SEM measurements and analysis. C.B. conducted the optical transmittance measurements and analysis. T.L. and Y.L. conducted the C-AFM measurements and analysis. M.N.L. conducted the EDX (SEM) measurements and analysis. J.P., D.J., K.J.W., K.R.C. and T.P.W. contributed to the results analysis and interpretation. The manuscript was mainly written and revised by J.P. and T.P.W. All authors contributed to the discussion of the results and commented on the manuscript.

Acknowledgements

This work was supported by the Australian Government through the Australian Renewable Energy Agency (ARENA) and the Australian Research Council. Responsibility for the views, information or advice expressed herein is not accepted by the Australian Government. W.Y., D.Z. and J.L. acknowledge funding from MSTC (Grant No. 2016YFA0301300), NNSFC (Grant No. 11674402) and GSTP (Grant Nos. 201607010044, 201607020023). The work was partly conducted at the ACT node of the Australian National Fabrication Facility (ANFF), and the ANU node of the Australian Microscopy and Microanalysis Facility (AMMRF). The authors thank X.Z. Zhou and J. Xiang for discussing the UPS measurements.

References

1 NREL chart, www.nrel.gov/ncpv/images/efficiency_chart.jpg, (accessed: April 2017)

2 W. S. Yang, J. H. Noh, N. J. Jeon, Y. C. Kim, S. Ryu, J. Seo and S. I. Seok, *Science*, 2015, **348**, 1234-1237.

3 H. Tan, A. Jain, O. Voznyy, X. Lan, F. P. G. de Arquer, J. Z. Fan, R. Quintero-Bermudez, M. Yuan, B. Zhang and Y. Zhao, *Science*, 2017, **355**, 722-726.

4 M. Saliba, T. Matsui, K. Domanski, J.-Y. Seo, A. Ummadisingu, S. M. Zakeeruddin, J.-P. Correa-Baena, W. R. Tress, A. Abate and A. Hagfeldt, *Science*, 2016, **354**, 206-209.

5 X. Li, D. Bi, C. Yi, J. D. Decoppet, J. Luo, S. M. Zakeeruddin, A. Hagfeldt and M. Gratzel, *Science*, 2016, **353**, 58-62.

6 D. Bi, W. Tress, M. I. Dar, P. Gao, J. Luo, C. Renevier, K. Schenk, A. Abate, F. Giordano, J. P. Correa Baena, J. D. Decoppet, S. M. Zakeeruddin, M. K. Nazeeruddin, M. Gratzel and A. Hagfeldt, *Sci. Adv.*, 2016, **2**, e1501170.

7 Q. Jiang, L. Zhang, H. Wang, X. Yang, J. Meng, H. Liu, Z. Yin, J. Wu, X. Zhang and J. You, *Nature Energy*, 2016, **2**, 16177.

8 C. Momblona, L. Gil-Escrig, E. Bandiello, E. M. Hutter, M. Sessolo, K. Lederer, J. Blochwitz-Nimoth and H. J. Bolink, *Energy Environ. Sci.*, 2016, **9**, 3456-3463.

9 F. Giordano, A. Abate, J. P. Correa Baena, M. Saliba, T. Matsui, S. H. Im, S. M. Zakeeruddin, M. K. Nazeeruddin, A. Hagfeldt and M. Graetzel, *Nat. Commun.*, 2016, **7**, 10379.

10 J. You, L. Meng, T.-B. Song, T.-F. Guo, Y. Yang, W.-H. Chang, Z. Hong, H. Chen, H. Zhou, Q. Chen, Y. Liu, N. De Marco and Y. Yang, *Nat. Nano.*, 2016, **11**, 75-81.

11 Z. Yu and L. C. Sun, *Adv. Energy Mater.*, 2015, **5**, 1500213.

12 S. S. Shin, W. S. Yang, J. H. Noh, J. H. Suk, N. J. Jeon, J. H. Park, J. S. Kim, W. M. Seong and S. I. Seok, *Nat. Commun.*, 2015, **6**, 7410.

13 H. Zhou, Q. Chen, G. Li, S. Luo, T.-b. Song, H.-S. Duan, Z. Hong, J. You, Y. Liu and Y. Yang, *Science*, 2014, **345**, 542-546.

14 J. T.-W. Wang, J. M. Ball, E. M. Barea, A. Abate, J. A. Alexander-Webber, J. Huang, M. Saliba, I. n. Mora-Sero, J. Bisquert and H. J. Snaith, *Nano Lett.*, 2013, **14**, 724-730.

15 S. S. Shin, E. J. Yeom, W. S. Yang, S. Hur, M. G. Kim, J. Im, J. Seo, J. H. Noh and S. I. Seok, *Science*, 2017, **356**, 167-171.

16 W. Tress, *Adv. Energy Mater.*, 2017, 1602358, DOI: 10.1002/aenm.201602358.

17 J.-P. Correa-Baena, W. Tress, K. Domanski, E. H. Anaraki, S.-H. Turren-Cruz, B. Roose, P. P. Boix, M. Grätzel, M. Saliba and A. Abate, *Energy Environ. Sci.*, 2017, DOI:10.1039/C7EE00421D

18 Y. Shao, Z. Xiao, C. Bi, Y. Yuan and J. Huang, *Nat. Commun.*, 2014, **5**, 5784.

19 C. Tao, S. Neutzner, L. Colella, S. Marras, A. R. S. Kandada, M. Gandini, M. De Bastiani, G. Pace, L. Manna, M. Caironi, C. Bertarelli and A. Petrozza, *Energy Environ. Sci.*, 2015, **8**, 2365-2370.

20 D. A. Jacobs, Y. Wu, H. Shen, C. Barugkin, F. J. Beck, T. P. White, K. Weber and K. R. Catchpole, *Phys. Chem. Chem. Phys.*, 2017, **19**, 3094-3103.

21 B. Chen, M. Yang, S. Priya and K. Zhu, *J. Phys. Chem. Lett.*, 2016, **7**, 905-917.

22 G. Richardson, S. E. O'Kane, R. G. Niemann, T. A. Peltola, J. M. Foster, P. J. Cameron and A. B. Walker, *Energy Environ. Sci.*, 2016, **9**, 1476-1485.

23 Y. Yang, M. Yang, D. T. Moore, Y. Yan, E. M. Miller, K. Zhu and M. C. Beard, *Nature Energy*, 2017, **2**, 16207.

24 Y. Hou, W. Chen, D. Baran, T. Stubhan, N. A. Luechinger, B. Hartmeier, M. Richter, J. Min, S. Chen and C. O. R. Quiroz, *Adv. Mater.*, 2016, **28**, 5112-5120.

25 M. Saliba, T. Matsui, J.-Y. Seo, K. Domanski, J.-P. Correa-Baena, M. K. Nazeeruddin, S. M. Zakeeruddin, W. Tress, A. Abate, A. Hagfeldt and M. Gratzel, *Energy Environ. Sci.*, 2016, **9**, 1989-1997.

26 S. K. Pathak, A. Abate, P. Ruckdeschel, B. Roose, K. C. Gödel, Y. Vaynzof, A. Santhala, S.-I. Watanabe, D. J. Hollman, N. Noel, A. Sepe, U. Wiesner, R. Friend, H. J. Snaith and U. Steiner, *Adv. Funct. Mater.*, 2014, **24**, 6046-6055.

27 J. Peng, T. Duong, X. Z. Zhou, H. P. Shen, Y. L. Wu, H. K. Mulmudi, Y. M. Wan, D. Y. Zhong, J. T. Li, T. Tsuzuki, K. J. Weber, K. R. Catchpole and T. P. White, *Adv. Energy Mater.*, 2017, **7**, 1601768.

28 E. H. Anaraki, A. Kermanpur, L. Steier, K. Domanski, T. Matsui, W. Tress, M. Saliba, A. Abate, M. Grätzel and A. Hagfeldt, J. P. Correa-Baena, *Energy Environ. Sci.*, 2016, **9**, 3128-3134.

29 J. P. Correa Baena, L. Steier, W. Tress, M. Saliba, S. Neutzner, T. Matsui, F. Giordano, T. J. Jacobsson, A. R. Srimath Kandada, S. M. Zakeeruddin, A. Petrozza, A. Abate, M. K. Nazeeruddin, M. Gratzel and A. Hagfeldt, *Energy Environ. Sci.*, 2015, **8**, 2928-2934.

30 C. L. Wang, D. W. Zhao, C. R. Grice, W. Q. Liao, Y. Yu, A. Cimaroli, N. Shrestha, P. J. Roland, J. Chen, Z. H. Yu, P. Liu, N. Cheng, R. J. Ellingson, X. Z. Zhao and Y. F. Yan, *J. Mater. Chem. A*, 2016, **4**, 12080-12087.

31 N. J. Jeon, J. Lee, J. H. Noh, M. K. Nazeeruddin, M. Gratzel and S. I. Seok, *J. Am. Chem. Soc.*, 2013, **135**, 19087-19090.

32 Z. Yuan, Z. Wu, S. Bai, Z. Xia, W. Xu, T. Song, H. Wu, L. Xu, J. Si, Y. Jin and B. Sun, *Adv. Energy Mater.*, 2015, **5**, 1500038.

33 T. Ye, S. Ma, X. Jiang, L. Wei, C. Vijila and S. Ramakrishna, *Adv. Funct. Mater.*, 2017, 1606545, DOI: 10.1002/adfm.201606545.

34 Q. Wang, Q. Dong, T. Li, A. Gruverman and J. Huang, *Adv. Mater.*, 2016, **28**, 6734-6739.

35 F. Zhang, W. Shi, J. Luo, N. Pellet, C. Yi, X. Li, X. Zhao, T. J. Dennis, X. Li, S. Wang, Y. Xiao, S. M. Zakeeruddin, D. Bi and M. Gratzel, *Adv. Mater.*, 2017, 1606806, DOI: 10.1002/adma.201606806

36 C. Tao, J. Van Der Velden, L. Cabau, N. F. Montcada, S. Neutzner, S. Kandada, A. Ram, S. Marras, L. Brambilla and M. Tommasini, *Adv. Mater.*, 2017, **29**, 1604493.

37 D. Koushik, W. J. H. Verhees, Y. H. Kuang, S. Veenstra, D. Zhang, M. A. Verheijen, M. Creatore and R. E. I. Schropp, *Energy Environ. Sci.*, 2017, **10**, 91-100.

38 L. Zuo, Z. Gu, T. Ye, W. Fu, G. Wu, H. Li and H. Chen, *J. Am. Chem. Soc.*, 2015, **137**, 2674-2679.

39 F. Wang, A. Shimazaki, F. Yang, K. Kanahashi, K. Matsuki, Y. Miyauchi, T. Takenobu, A. Wakamiya, Y. Murata and K. Matsuda, *J. Phys. Chem. C*, 2017, **121**, 1562-1568.

40 D. Bi, C. Yi, J. Luo, J.-D. Décoppet, F. Zhang, S. M. Zakeeruddin, X. Li, A. Hagfeldt and M. Grätzel, *Nature Energy*, 2016, **1**, 16142.

41 D.-Y. Son, J.-W. Lee, Y. J. Choi, I.-H. Jang, S. Lee, P. J. Yoo, H. Shin, N. Ahn, M. Choi and D. Kim, *Nature Energy*, 2016, **1**, 16081.

42 X. Dai, Z. Zhang, Y. Jin, Y. Niu, H. Cao, X. Liang, L. Chen, J. Wang and X. Peng, *Nature*, 2014, **515**, 96-99.

43 S. Song, W.-K. Hong, S.-S. Kwon and T. Lee, *Appl. Phys. Lett.*, 2008, **92**, 263109.

44 W. Kong, T. Ding, G. Bi and H. Wu, *Phys. Chem. Chem. Phys.*, 2016, **18**, 12626-12632.

45 N. K. Noel, A. Abate, S. D. Stranks, E. S. Parrott, V. M. Burlakov, A. Goriely and H. J. Snaith, *ACS Nano*, 2014, **8**, 9815-9821.

46 P.-W. Liang, C.-C. Chueh, S. T. Williams and A. K. Y. Jen, *Adv. Energy Mater.*, 2015, **5**, 1402321.

47 C. H. Chiang and C. G. Wu, *Nat. Photon.*, 2016, **10**, 196-200.

48 C. J. Brabec, S. Gowrisanker, J. J. M. Halls, D. Laird, S. Jia and S. P. Williams, *Adv. Mater.*, 2010, **22**, 3839-3856.
49 P. Wurfel, *J. Phys. C Solid State Phys.*, 1982, **15**, 3967-3985.
50 G. Smestad and H. Ries, *Sol. Energy Mater. Sol. Cells*, 1992, **25**, 51-71.
51 Y. Wu, H. Shen, D. Walter, D. Jacobs, T. Duong, J. Peng, L. Jiang, Y.-B. Cheng and K. Weber, *Adv. Funct. Mater.*, 2016, **26**, 6807-6813.
52 H. Yu, H. P. Lu, F. Y. Xie, S. Zhou and N. Zhao, *Adv. Funct. Mater.*, 2016, **26**, 1411-1419.
53 I. Levine, P. K. Nayak, J. T.-W. Wang, N. Sakai, S. Van Reenen, T. M. Brenner, S. Mukhopadhyay, H. J. Snaith, G. Hodes and D. Cahen, *J. Phys. Chem. C*, 2016, **120**, 16399-16411.
54 A. Baumann, K. Tvingstedt, M. Heiber, S. Väth, C. Momblona, H. Bolink and V. Dyakonov, *APL Materials*, 2014, **2**, 081501.
55 F. Huang, L. Jiang, A. R. Pascoe, Y. Yan, U. Bach, L. Spiccia and Y.-B. Cheng, *Nano Energy*, 2016, **27**, 509-514.